

Multistage cooling and freezing of a saline spherical water droplet

A.R. Dehghani-Sanij^{a,b,*}, S. MacLachlan^c, G.F. Naterer^a, Y.S. Muzychka^a, R.D. Haynes^c, V. Enjilela^d

^a Department of Mechanical Engineering, Memorial University of Newfoundland, St. John's, NL, A1B 3X5, Canada

^b Waterloo Institute for Sustainable Energy (WISE), University of Waterloo, Waterloo, ON, Canada

^c Department of Mathematics and Statistics, Memorial University of Newfoundland, St. John's, NL, A1C 5S7, Canada

^d Department of Mechanical Engineering, Faculty of Mechatronics, Karaj Branch, Islamic Azad University, Karaj, Iran

ARTICLE INFO

Keywords:

Water droplet
Moving boundary problem
Semi-analytical technique
Phase change
Solidification

ABSTRACT

In this paper, the thermal behaviour of a saline water droplet during flight over a marine vessel in cold weather conditions is investigated by analytical and semi-analytical techniques. To predict and analyze the droplet cooling and freezing processes, three stages are employed: a liquid cooling stage, a solidification stage, and a solid cooling stage. The theoretical model considers heat transfer via conduction inside the droplet as well as convection, evaporation (just for the liquid cooling stage), and radiation heat transfer from the droplet's surface to the ambient air. A novel semi-analytical solution technique is developed to analyze the inward moving boundary problem for the solidification stage. The results show that the liquid cooling stage is very short, and the temperature at the droplet's center remains close to the initial droplet temperature. During the solidification stage, the velocity of the inward freezing front within the droplet is approximately constant, and the temperature variations are linear when the temperature inside the droplet reaches the freezing temperature. The solid cooling stage is much longer than the other stages, and the temperature changes are non-linear. For a case study, theoretical predictions show that the average temperature of a droplet with a diameter of 1 mm at the moment of impact on the deck is approximately -1.95°C . Moreover, there is an ice shell with a thickness of 0.06 mm on the surface of the water droplet at the moment of impact.

1. Introduction

Solidification and melting processes have a wide range of practical applications such as thermal energy storage systems; freezing foods; crystal growth; laser glazing; ice formation on power cables; marine platforms and aircraft; processing of metals and alloys (e.g., casting and welding); groundwater freezing; low-temperature biology; and medicine [1–6]. The trajectory, cooling and freezing of water droplets in cold climates are important issues for modeling and prediction of sea spray icing phenomena on marine vessels and offshore structures [7–14]. During the harsh environmental conditions in cold seas and ocean areas, sea spray icing is created by wind-induced spray and wave-induced spray because of the impingement of waves at the bow of marine vessels and/or the base of offshore structures [7–14]. Fig. 1 illustrates the evolution of seawater spray and the motion of a spray cloud over a marine vessel. It is reported that sea spray icing can pose substantial challenges to marine operations, such as a serious threat to the stability of marine platforms and the safety of the crew [9–13,15].

The freezing process of water droplets in cold weather conditions corresponds with a phase change from liquid to solid. This phase change, or Stefan problem, is a moving boundary problem, which is non-linear and typically cannot be solved analytically. Thus, numerical and approximate methods are generally used to solve these types of problems. Neumann [16] found an exact solution for one-dimensional solidification in a semi-infinite region that is not initially at the fusion temperature. Neumann's solution led to a small number of exact similarity solutions. For several cases, such as finite domains, with two phases present initially, non-uniform initial temperatures, and boundary temperatures that are arbitrary functions of time, similarity methods cannot be used to find the exact solutions [17]. While approximate methods are an obvious alternative, Schulze et al. [18] stated that these are commonly not sufficiently accurate for problems with short time scales. Hindmarsh et al. [19] reported several numerical techniques that have been formulated to solve moving boundary problems. These numerical techniques include the "temperature formulation" by Murray and Landis [20], the "enthalpy formulation" by Voller [21], the "heat balance integral methods" by Caldwell and Chan [22], the "equivalent

* Corresponding author. Department of Mechanical Engineering, Memorial University of Newfoundland, St. John's, NL, A1B 3X5, Canada.

E-mail addresses: adehghani@mun.ca, a7degha@uwaterloo.ca (A.R. Dehghani-Sanij).

Different assumptions are commonly used to solve the inward spherical freezing problem using perturbation techniques, including: constant thermophysical properties [4–6,26–31,36], equal values for the densities of liquid and solid phases [2,4,35], and a constant freezing temperature with the liquid uniformly at the freezing temperature [27]. In the present study, a novel semi-analytical solution technique is utilized to investigate the one-dimensional inward moving boundary problem for the solidification stage. In this solution, a semi-discretization method in time and separation of variables method in the radial direction are employed to determine the temperature distribution within a saline water droplet.

Tabakova et al. [2] studied the freezing process of a spherical droplet by considering two different stages: “recalescence” and a phase change process to/from solidification. To analyze and solve the problem, they used two distinct methods: (a) the technique of matched asymptotic expansions for a small Stefan number and an arbitrary Biot number, as well as (b) a numerical approach for an arbitrary Stefan number, employing an enthalpy method. Their results showed good agreement between the two methods. Feuillebois et al. [35] reported three possible locations where ice accretion can occur in the recalescence stage, including: (1) at the center of the droplet, (2) a uniform distribution formed randomly within the droplet, and (3) at the outside surface of the droplet.

The heat and mass transfer from a single water droplet and a system of droplets was studied by Zarling [37], who neglected heat conduction within the droplet and considered convection, evaporation and radiation heat transfer from the surface of the droplet. Hindmarsh et al. [38] experimentally and numerically investigated the temperature behaviour during the solidification of a food solution droplet. They considered five different stages for the solidification of the droplet: liquid cooling and supercooling, nucleation, recalescence, freezing, and solid cooling or tempering. In another study, Hindmarsh et al. [19] analyzed the freezing process of a suspended water droplet using numerical and experimental methods. They studied both outward and inward moving boundaries during the solidification process of the droplet. Results showed that the outward solidification model predicted shorter freezing times compared to the inward solidification model. In the present study, the model used is similar to the model considered by Hindmarsh et al. [19,38]; however, we propose a novel semi-analytical technique to solve the moving boundary problem.

The objective of this paper is to predict and analyze the cooling and solidification processes of a saline water droplet in cold weather conditions during its flight over a marine vessel. Three separate stages are considered for modeling and prediction of the cooling and freezing processes of the water droplet. By considering heat conduction within the droplet as well as convection, evaporation (just for the liquid cooling stage), and radiation heat transfer from the droplet’s surface, the thermal behaviour of the droplet is investigated using analytical and semi-analytical techniques. According to the literature, the semi-analytical technique, which has been used in this study, is a novel approach to find an approximate solution for the moving boundary problems. Additionally, the influence of different parameters on the droplet cooling and solidification processes is investigated.

2. Model description

To analyze and predict the cooling and freezing processes of a saline water droplet during flight on a marine vessel, two cases can be considered: (1) a uniform temperature within the droplet, and (2) heat conduction and a temperature gradient within the droplet. The authors consider the latter case herein. Three different stages during the cooling and freezing processes are considered. In the first stage, or the liquid cooling stage, the droplet is fully liquid and its volume will decrease because of evaporation from the droplet’s surface. The second stage, or solidification stage, will begin when the surface temperature reaches the freezing temperature, and an ice shell will form on the surface of the

droplet. A number of experimental investigations have illustrated that solidification in droplets generally occurs from the surface by forming a frozen shell that expands towards the center of the droplets [1,19,39,40]. Hence, inward freezing for the spherical saline water droplet is considered. In the third stage, or solid cooling stage, the droplet and its salt content will freeze completely. A brine-spongy ice will form, which contains pure ice, brine pockets and air bubbles. Fig. 2 displays the variations of a saline water droplet in the different stages of freezing when the droplet moves over a marine vessel.

2.1. Droplet trajectory model

To determine the rate of heat and mass transfer from the water droplet, the trajectory and velocity of the droplet must be calculated. Several forces affect the droplet’s movement throughout its flight in the ambient air, including the drag force, body forces (gravity and buoyancy) and added mass force [7,8,41–48]. In this paper, only the air drag and gravity forces are considered to specify the water droplet trajectory. Thus, the motion of the droplet is governed by [41,42,45,48]:

$$\frac{d\vec{v}_d}{dt} = -\frac{3}{4} \frac{C_d}{D} \frac{\rho_a}{\rho_d} |\vec{v}_d - \vec{U}| (\vec{v}_d - \vec{U}) - \vec{g} \left(\frac{\rho_a}{\rho_d} - 1 \right) \quad (1)$$

Here, v_d is the droplet velocity relative to the ground, t is the time, C_d is the droplet’s drag coefficient, D is the droplet diameter, ρ_a is the density of the air, ρ_d is the density of the water droplet (assumed to be equal to the seawater density), g is the gravitational acceleration and U is the wind velocity. The droplet’s drag coefficient can be estimated by [49]:

$$C_d = \begin{cases} \frac{24.0}{Re} & , Re \leq 1 \\ \frac{24.0}{Re} (1 + 0.15 Re^{0.687}) & , 1 < Re \leq 1000 \\ 0.44 & , Re > 1000 \end{cases} \quad (2)$$

where Re is the droplet’s Reynolds number,

$$Re = \frac{D u_{eff}}{\nu_a} \text{ and } u_{eff} = |\vec{v}_d - \vec{U}| \quad (3)$$

Here, u_{eff} is the effective velocity and ν_a is the air kinematic viscosity. Dehghani et al. [7,8] conducted numerical studies to determine the trajectories and the distribution of sizes and velocities of water droplets, which arise due to wave-impact spray over a medium-size fishing vessel (MFV). Furthermore, they found the initial velocity of droplets with different sizes at the edge of the MFV. The initial velocities for the droplets with a diameter near zero and a diameter of 7 mm are 60 m/s and 0 m/s, respectively. Moreover, between these droplet diameters and initial velocities, there is almost a linear inverse relation. By combining Eqs. (1)–(3) and solving these equations with the use of a numerical time stepping technique, the droplet velocity relative to the ground can be computed.

In order to determine the position of the water droplet trajectories throughout their motion over the marine vessel depicted in Fig. 1, we use the following relationships [48]:

$$\frac{d^2x}{dt^2} = -\frac{3}{4} \frac{C_d}{D} \frac{\rho_a}{\rho_d} \left(\frac{dx}{dt} - U_{rw} \right) \sqrt{\left(\frac{dx}{dt} - U_{rw} \right)^2 + \left(\frac{dy}{dt} \right)^2} \quad (4)$$

$$\frac{d^2y}{dt^2} = g \left(\frac{\rho_a}{\rho_d} - 1 \right) - \frac{3}{4} \frac{C_d}{D} \frac{\rho_a}{\rho_d} \left(\frac{dy}{dt} \right) \sqrt{\left(\frac{dx}{dt} - U_{rw} \right)^2 + \left(\frac{dy}{dt} \right)^2} \quad (5)$$

where x and y are the components of the positions of water droplets relative to the vessel and U_{rw} is the velocity of wind relative to the vessel. The effects of evaporation on the droplet mass are neglected [8,48]. To solve Eqs. (4) and (5), we utilize the following initial conditions:

$$x(t = 0) = 0 \tag{6}$$

$$\frac{dx}{dt} (t = 0) = v_{d0,x} = v_{d0} \cos \delta \tag{7}$$

$$y(t = 0) = 0 \tag{8}$$

$$\frac{dy}{dt} (t = 0) = v_{d0,y} = v_{d0} \sin \delta \tag{9}$$

where v_{d0} is the initial droplet velocity and δ is the initial travel angle of the water droplets.

2.2. Heat transfer model

As in Fig. 2, the water droplet cools due to convection, evaporation and radiation heat transfer within the airflow. The convective heat loss with the ambient air can be calculated by [42]:

$$Q_c = h_c (T_d - T_a) \tag{10}$$

$$h_c = \frac{Nu k_a}{D} \tag{11}$$

$$Nu = 2.0 + 0.6 Pr^{0.33} Re^{0.5} \tag{12}$$

where h_c is the convection heat transfer coefficient of the droplet, T_d is the droplet temperature, T_a is the air temperature, k_a is the thermal conductivity of the air, Nu is the droplet's Nusselt number, and Pr is the Prandtl number of the airflow. It should be noted that in the above equations, the Reynolds number (Re) and subsequently the convective heat loss (Q_c) are dependent on the droplet velocity (v_d), which is described in the previous subsection. The parameter Pr is given by:

$$Pr = \frac{\mu_a}{\rho_a \alpha_a} \tag{13}$$

Here, α_a is the thermal diffusivity of the air and μ_a is the dynamic viscosity of the air, which is given by [50]:

$$\mu_a = \mu_o \left[\frac{T_o + 120}{T + 120} \left(\frac{T}{T_o} \right)^{1.5} \right] \tag{14}$$

where $\mu_o = 1.8325 \times 10^{-5} Pa.s$, $T_o = 296.16 K$ and $T = (T_a + 273.15) K$. Also, the air density ρ_a , is expressed by [50]:

$$\rho_a = \frac{P}{287.04 (T_a + 273.15)} \tag{15}$$

where P is the atmospheric air pressure and T_a is in units of °C.

The evaporative heat loss with the ambient air can be computed by [51]:

$$Q_e = h_c \left(\frac{Pr}{Sc} \right)^{0.63} \frac{\epsilon l_v}{P c_a} (e_s(T) - RH \cdot e_s(T_a)) = C (e_s(T) - RH \cdot e_s(T_a)) \tag{16}$$

Here, Sc is the droplet's Schmidt number, ϵ is the ratio of the molecular weight of water vapour and dry air, l_v is the latent heat of vaporization of water, c_a is the specific heat capacity of dry air at a constant pressure, RH is the relative humidity of the air, and $e_s(T)$ is the saturated vapour pressure, which is linearized by [52]:

$$e_s(T) \approx E_0 + e_0 T \tag{17}$$

where $e_0 = 27.03 Pa/K$ and $E_0 = - 6803 Pa$. In addition, the droplet's Schmidt number is estimated by:

$$Sc = \frac{\mu_a}{\rho_a D_{ab}} \tag{18}$$

Here, D_{ab} is the air-water vapour diffusivity.

The heat loss because of long-wave radiation can be obtained by:

$$Q_r = \epsilon \sigma (T_d^4 - T_a^4) \tag{19}$$

where ϵ is the droplet emissivity and σ is the Stefan-Boltzmann constant. The above equation can be simplified using the radiation heat transfer coefficient of the droplet, h_r , which is determined by:

$$h_r = \epsilon \sigma (T_d^2 + T_a^2) (T_d + T_a) \tag{20}$$

Zarling [37] reported that when the temperature differences are not large, the radiation heat transfer coefficient can be approximated as a constant, or by using the following relationship:

$$h_r = \epsilon \sigma (T_{0,w}^2 + T_a^2) (T_{0,w} + T_a) \tag{21}$$

where $T_{0,w}$ is the initial temperature of the droplet. Therefore, Eq. (19) can be written as:

$$Q_r = h_r (T_d - T_a) \tag{22}$$

A number of assumptions will be employed in order to analytically solve the problem, including: (1) the initial temperature of the droplet in a spray event is equal to the temperature of the water's surface, (2) the volume and distribution of brine pockets and air bubbles as well as the concentration of brine pockets inside the ice shell is uniform, (3) the properties of ice formation, such as the thermal conductivity, density and the specific heat capacity, are uniform in the ice shell, and (4) the velocity of wind is uniform and in the horizontal direction.

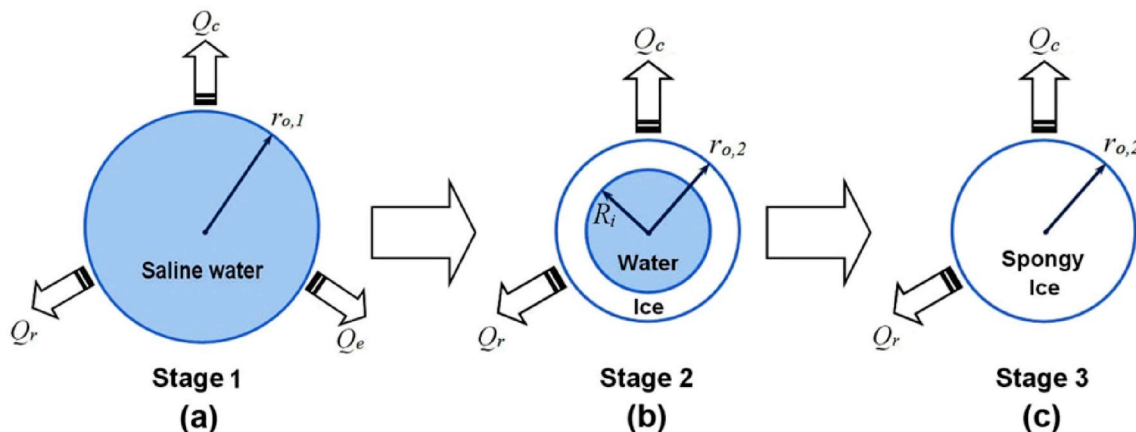


Fig. 2. Schematic of the changes of a saline water droplet in freezing conditions during motion over a marine vessel.

2.3. Droplet cooling and freezing processes

The governing equation in spherical coordinates can be written as [53,54]:

$$\frac{\partial(\rho c T)}{\partial t} = \frac{1}{r^2} \frac{\partial}{\partial r} \left(k r^2 \frac{\partial T}{\partial r} \right), \quad 0 \leq r \leq r_d \quad (23)$$

where ρ is the density, c is the specific heat capacity, k is the thermal conductivity, T is the temperature, and r is the radial coordinate. In this study, the origin of the coordinate system is located in the center of the droplet. To solve Eq. (23) for each stage, boundary and initial conditions are needed. These boundary and initial conditions will be explained in the following subsections.

2.3.1. Liquid cooling stage (stage 1)

By symmetry, the boundary condition at the center of the saline water droplet is given by:

$$\frac{\partial T_w}{\partial r} \left(r = 0 \right) = 0 \quad (24)$$

To determine the boundary condition at the surface of the droplet, we consider conduction heat transfer within the droplet as well as convection, evaporation, and radiation heat transfer (as derived in subsection 2.2) between the droplet's surface and the ambient air. We make use of an averaged value of the convection heat transfer coefficient of the droplet, h_c , to avoid solving with a time-dependent boundary condition, noting that the liquid cooling stage is very short so such an average is reasonable. This yields:

$$k_b \frac{\partial T_w}{\partial r} \left(r = r_{o,1} \right) = - (Q_c + Q_e + Q_r) \quad (25)$$

By substituting Q_c , Q_e and Q_r into Eq. (25), the equation below will be obtained:

$$\frac{\partial T_w}{\partial r} \left(r = r_{o,1} \right) = G_2 - G_1 T_w \left(r = r_{o,1} \right) \quad (26)$$

where the coefficients G_1 and G_2 are defined as:

$$G_1 = \frac{(h_c + h_r + C e_0)}{k_b} \quad (27)$$

$$G_2 = \frac{[(h_c + h_r + C RH e_0) T_a + C E_0 (RH - 1)]}{k_b} \quad (28)$$

The initial condition for the first stage is:

$$T_w(r, 0) = T_{0,w} \quad (29)$$

The variations in the droplet's radius during the cooling stage can be determined by solving the following equation [48,54–56].

$$(4 \pi r^2) \frac{dr}{dt} = - \frac{\dot{m}_v}{\rho_b} \quad (30)$$

where \dot{m}_v is the evaporation rate from the droplet's surface to the ambient air, which is given by [48,57]:

$$\dot{m}_v = \frac{Q_e}{l_v} \quad (31)$$

It is assumed that the change of the droplet's volume during the first stage is negligible. Dehghani-Sanij et al. [48] reported that the decrease in droplet size owing to evaporation during the droplet motion over a marine vessel is very small.

2.3.2. Solidification stage (stage 2)

When the temperature of the droplet's surface reaches the freezing temperature, the first particles of ice form on the top and bottom surfaces (when the droplet moves in the horizontal direction), because of a higher wind velocity, and then there is the ice growth to cover other portions of the droplet. Subsequently, an ice shell will be created on the entire surface of the droplet. Throughout the solidification stage, the internal liquid progressively varies from water to ice, and the latent heat of fusion must be transferred to the ambient air via the ice shell. It is assumed that growth of the ice shell within the droplet is uniform during the solidification stage; however, in practice, there are different shapes of freezing. Fig. 3 illustrates the freezing process of the water droplet in the second stage.

In accordance with Fig. 2(b), the boundary conditions for the water and ice shell are:

$$\frac{\partial T_w}{\partial r} \left(r = 0 \right) = 0 \quad (32)$$

$$-k_i \frac{\partial T_i}{\partial r} \left(r = r_{o,2} \right) = (h_c + h_r) [T_i(r = r_{o,2}) - T_a] \quad (33)$$

$$T_w(R_i, t) = T_i(R_i, t) = T_f \quad (34)$$

where T_f is the freezing temperature at the water-ice interface and the subscripts w and i refer to the water and ice shell, respectively. Note that evaporation from the droplet's surface in the second stage is negligible [48].

By applying a phase change or Stefan condition at the ice-water interface, the following equation is obtained:

$$\rho_i l_f (1 - \beta) \frac{dR_i}{dt} = k_i \frac{\partial T_i}{\partial r} \left(r = R_i \right) - k_b \frac{\partial T_w}{\partial r} \left(r = R_i \right) \quad (35)$$

Here, l_f is the latent heat of fusion of pure ice, $l_f (1 - \beta)$ is the latent heat of fusion of the saline ice formation [58,59] and β is the interfacial distribution coefficient. Note that the radius of the freezing interface, R_i , is a function of time, which varies between 0 and the radius of the droplet in the solidification stage.

The initial conditions for the water and ice shell, respectively, are:

$$T_w(r, 0) = T_1 \quad (36)$$

$$T_i(r = r_{o,2}, 0) = T_f \quad (37)$$

where T_1 is the temperature obtained from the liquid cooling stage at the freezing time, t_f .

Forest et al. [60], based on a study conducted by Assur [61], obtained a more accurate relation between brine salinity, S_b , and freezing temperature, T_f , for three temperature regions. The relation for the first region is:

$$T_f = -54.1126 \left(\frac{S_b}{1 - S_b} \right), \quad -7.7 \leq T_f \leq 0^\circ C \text{ and } 0 \leq S_b \leq 124.7\text{‰} \quad (38)$$

The relation for the second region is:

$$T_f = \frac{0.063 - 1.063 S_b}{0.01031 (1 - S_b)}, \quad -23 \leq T_f < -7.7^\circ C \text{ and } 124.7 < S_b \leq 230.8\text{‰} \quad (39)$$

and the relation for the third region is:

$$S_b = \frac{3.3136 \times 10^{-4} T_f^2 + 0.01524 T_f + 0.4752}{3.3136 \times 10^{-4} T_f^2 + 0.01524 T_f + 1.4752}, \quad -36 \leq T_f < -23^\circ \text{C} \text{ and } 230.8 < S_b \leq 262.5\% \quad (40)$$

The brine salinity, S_b , appears as a fraction in the above formulae.

The salinity has an effect on several parameters, such as the density, thermal conductivity, specific heat capacity, and freezing temperature. Andreas [62] reported that the salinity of seawater spray will increase due to evaporation and the equilibrium radius of a water droplet is one-half of the radius at its formation for a relative humidity of 80%. Kulyakhtin and Tsarau [41] found that the salinity of a water droplet created by wave spray is equal to the seawater salinity, but the salinity of a droplet produced by wind spray is higher than the seawater salinity. Schwerdtfeger [63] reported that the highest amount of salt in unfrozen water is equal to 237‰ when the temperature is -17°C [41]. Horjen [57] reported that the droplet salinity for large water droplets, from impact-generated sea spray, is only slightly higher than the seawater surface salinity because of evaporation during flight. However, for water droplets with small sizes (about 0.1 mm) and also long flight distances, the difference between the droplet salinity and seawater salinity is significant. In the present study, consider the droplet salinity, S_b , to be equal to the seawater salinity, S_w , when the droplet diameter is equal to or greater than 0.5 mm.

2.3.3. Solid cooling stage (stage 3)

Following Fig. 2(c), the boundary and initial conditions for the solid cooling stage are:

$$\frac{\partial T_i}{\partial r}(r=0) = 0 \quad (41)$$

$$-k_i \frac{\partial T_i}{\partial r}(r=r_{o,2}) = (h_c + h_r)[T_i(r=r_{o,2}) - T_a] \quad (42)$$

$$T_i(r=r_{o,2}, 0) = T_2 \quad (43)$$

where T_2 is the temperature obtained from the freezing stage at the solidification time, t_s . During this stage, evaporation from the droplet's surface is neglected [48].

3. Solution procedure

This section investigates and analyzes the one-dimensional inward moving boundary problem for the solidification of a saline water droplet

using analytical and semi-analytical techniques, which is the main contribution of this study. To find the temperature distribution within the droplet at the various stages, the solution procedure will be outlined in the following sub-sections. It should be noted that while the solution procedure for the liquid and solid cooling stages is quite standard, a new semi-analytical technique for the solidification stage is proposed, making use of a discrete approximation of the Stefan condition to time-step an approximate solution.

3.1. Solution procedure for the liquid cooling stage

To determine the temperature distribution inside the water droplet in the liquid cooling and solid cooling stages, an analytical technique can be used. By using the separation of variables method [64] and applying the boundary and initial conditions (Eqs. (24), (26) and (29)), the solution for the temperature distribution in the liquid cooling stage can be written as:

$$T_w(r, t) = \frac{G_2}{G_1} + \sum_{n=1}^{\infty} A_n \frac{\sin(\lambda_n r)}{r} \exp(-\alpha_b \lambda_n^2 t) \quad (44)$$

where α_b is the thermal diffusivity of brine,

$$\alpha_b = \frac{k_b}{\rho_b c_b} \quad (45)$$

and A_n is a coefficient defined by:

$$A_n = \frac{\left(T_{0,w} - \frac{G_2}{G_1}\right) \left[\frac{1}{\lambda_n^2} \sin(\lambda_n r_{o,1}) - \frac{r_{o,1}}{\lambda_n} \cos(\lambda_n r_{o,1})\right]}{\frac{r_{o,1}}{2} - \frac{1}{4\lambda_n} \sin 2(\lambda_n r_{o,1})} \quad (46)$$

The eigenvalues, λ_n , are determined from the positive roots of the transcendental equation:

$$\tan(\lambda_n r_{o,1}) = \frac{\lambda_n}{\left(\frac{1}{r_{o,1}} - G_1\right)} \quad (47)$$

To estimate the density of brine ρ_b , the following formula is used [57]:

$$\rho_b = 1000 + 0.8 S_b \quad (48)$$

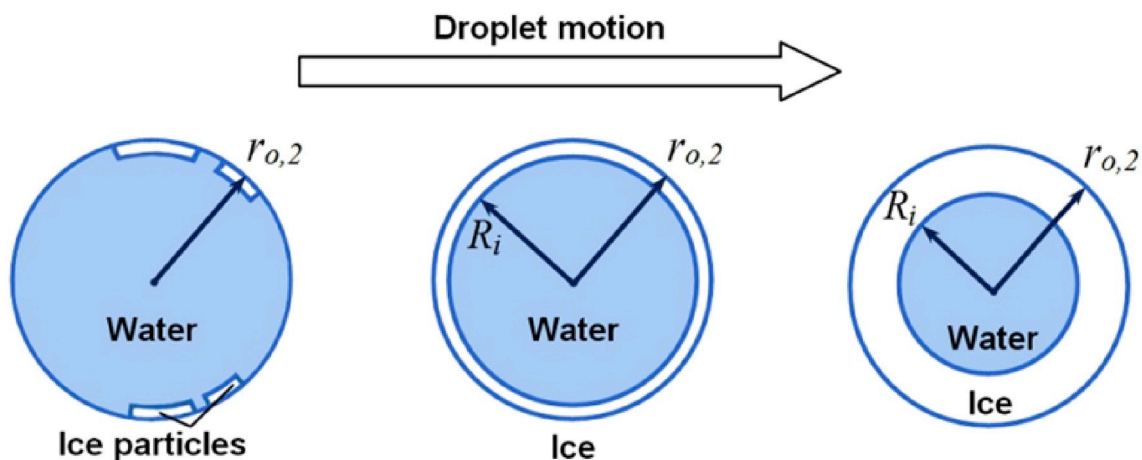


Fig. 3. Schematic of the solidification process of a saline water droplet in the second stage.

The thermal conductivity of brine, k_b , can be computed by [65,66]:

$$k_b = 0.523 + 0.013 T_b \quad (49)$$

where T_b is the brine temperature ($^{\circ}C$), which is given by [61]:

$$T_b = -\frac{a S_b}{1 - 10^{-3} S_b}, \quad S_b < 125\% \quad (50)$$

$$T_b = -\frac{b S_b}{1 - 10^{-3} S_b} + c, \quad 125\% \leq S_b < 230\% \quad (51)$$

Here, $a = 5.4113 \times 10^{-2} \text{ }^{\circ}C$, $b = 9.7007 \times 10^{-2} \text{ }^{\circ}C$ and $c = 6.0533 \text{ }^{\circ}C$.

Kuwahara [67] reported an experimental relationship to determine the specific heat capacity of seawater at $0^{\circ}C$ and atmospheric pressure, which is equal to:

$$c_b = 1.005 - 0.004136 S_b + 0.0001098 S_b^2 - 0.000001324 S_b^3 \quad (52)$$

In this relationship, c_b is in units of $Cal/gr. ^{\circ}C$.

In practice, a truncated form of the series solution in Eq. (44) is used, with 10 terms. The eigenvalues, λ_n , are computed numerically using the bisection method.

3.2. Solution procedure for the solidification stage

In the solidification stage, there is a phase change or Stefan-type condition. A semi-analytical technique is introduced to evolve the moving boundary problem inside the water droplet. In this technique, a semi-discretization method in time and separation of variables method in the radial direction are used to compute the temperature distribution in the water and the ice shell.

In order to homogenize the boundary conditions in the water, a temperature excess $\theta_w = T_w - T_f$, is used. Thus, the governing equation can be written as:

$$B_{m,k} = \sum_{n=1}^{\infty} B_{n,k-1} \frac{R_i^{k-1}}{\pi \left(1 + \Delta t \alpha_b \left(\frac{m\pi}{R_i^k}\right)^2\right)} \left\{ \left(\frac{1}{(n R_i^k - m R_i^{k-1})} \sin \left(\pi \left(\frac{n R_i^k - m R_i^{k-1}}{R_i^{k-1}} \right) \right) \right) - \left(\frac{1}{(n R_i^k + m R_i^{k-1})} \sin \left(\pi \left(\frac{n R_i^k + m R_i^{k-1}}{R_i^{k-1}} \right) \right) \right) \right\} \quad (63)$$

$$\frac{1}{r^2} \frac{\partial}{\partial r} \left(r^2 \frac{\partial \theta_w}{\partial r} \right) = \frac{1}{\alpha_b} \frac{\partial \theta_w}{\partial t}, \quad 0 \leq r < R_i \quad (53)$$

which is subject to:

$$\frac{\partial \theta_w}{\partial r} \left(r = 0 \right) = 0 \quad (54)$$

$$\theta_w(R_i, t) = 0 \quad (55)$$

$$\theta_w(r, 0) = T_1 - T_f \quad (56)$$

Note that the initial condition is specifically $T_1(r) = T_w(r, t_f)$, using the solution from the cooling stage in Eq. (44) at time t_f , when freezing begins. In Eq. (53), R_i is the interface radius, which changes with time during the solidification stage. Applying the separation of variables method yields a series solution of the form:

$$\theta_w(r, t) = \sum_{n=1}^{\infty} B_n(t) \frac{\sin\left(\frac{n\pi}{R_i} r\right)}{r}, \quad 0 \leq r < R_i \quad (57)$$

In the above equation, R_i is not fixed because it changes with time;

thus, the separation of variables method cannot be applied in the usual way. Instead, approximate the time derivative by:

$$\frac{\partial \theta_w}{\partial t}(r, t_k) \simeq \frac{\theta_w(r, t_k) - \theta_w(r, t_k - \Delta t)}{\Delta t} \quad (58)$$

Using this, Eq. (53) can then be approximated as follows:

$$\theta_w(r, t_k) = \theta_w(r, t_k - \Delta t) + \Delta t \frac{\alpha_b}{r^2} \frac{\partial}{\partial r} \left(r^2 \frac{\partial \theta_w}{\partial r}(r, t_k) \right) \quad (59)$$

Taking $B_{n,k} = B_n(t_k)$ and the interface radius at time t_k to be $R_i^k = R_i(t_k)$, we write:

$$\theta_w(r, t_k) = \sum_{n=1}^{\infty} B_{n,k} \frac{\sin\left(\frac{n\pi}{R_i^k} r\right)}{r} \quad (60)$$

and

$$\theta_w(r, t_k - \Delta t) = \sum_{n=1}^{\infty} B_{n,k-1} \frac{\sin\left(\frac{n\pi}{R_i^{k-1}} r\right)}{r} \quad (61)$$

Now, substituting Eqs. (60) and (61) into Eq. (59), the following relationship is obtained.

$$\sum_{n=1}^{\infty} \left(1 + \Delta t \alpha_b \left(\frac{n\pi}{R_i^k} \right)^2 \right) B_{n,k} \frac{\sin\left(\frac{n\pi}{R_i^k} r\right)}{r} = \sum_{n=1}^{\infty} B_{n,k-1} \frac{\sin\left(\frac{n\pi}{R_i^{k-1}} r\right)}{r} \quad (62)$$

During solidification, the interface radius is decreasing in time, that

is $R_i^k < R_i^{k-1}$. Multiplying by $\frac{\sin\left(\frac{m\pi}{R_i^k} r\right)}{r}$ in the above relationship and integrating from 0 to R_i^k , the coefficients $B_{m,k}$ can be determined as:

To complete the calculation of the coefficients, $B_{m,k}$, the initial condition, Eq. (56) must be applied. Using the initial condition, we find:

$$B_{m,1} = \left(T_f - \frac{G_2}{G_1} \right) \left[\frac{2R_i^1}{m\pi} (-1)^m \right] + \sum_{n=1}^{\infty} A_n \frac{1}{R_i^1} \left\{ \left(\frac{1}{\left(\lambda_n - \frac{m\pi}{R_i^1} \right)} \sin \left(\left(\lambda_n - \frac{m\pi}{R_i^1} \right) R_i^1 \right) \right) - \left(\frac{1}{\left(\lambda_n + \frac{m\pi}{R_i^1} \right)} \sin \left(\left(\lambda_n + \frac{m\pi}{R_i^1} \right) R_i^1 \right) \right) \right\} \exp(-\alpha_b \lambda_n^2 t_f) \quad (64)$$

where R_i^1 is the radius of the droplet at the start of the solidification stage, that is $R_i^1 = r_{o,2}$. After computing $B_{m,1}$ from Eq. (64), the coefficients $B_{m,k}$ can be computed for all t_k if R_i^k is known. Consequently, the solution for the temperature distribution in the water can be written as:

$$\theta_w(r, t_k) = \sum_{m=1}^{\infty} B_{m,k} \frac{\sin\left(\frac{m\pi}{R_i^k} r\right)}{r}, \quad 0 \leq r < R_i \quad (65)$$

In practice, a truncated version of the series solution is used.

To find the temperature distribution in the ice shell, a similar semi-analytical solution procedure will be used. To homogenize the boundary conditions in the ice shell, a temperature excess $\theta_i = T_i - (a + br)$, is introduced. Applying homogeneous boundary conditions, the parameters a and b can be calculated as:

$$a = T_f - \frac{(T_a - T_f)R_i}{\left[r_{o,2} - R_i + \left(\frac{k_i}{h_c + h_r}\right)\right]} \quad (66)$$

$$b = \frac{(T_a - T_f)}{\left[r_{o,2} - R_i + \left(\frac{k_i}{h_c + h_r}\right)\right]} \quad (67)$$

The governing equation for the ice shell can then be written as follows:

$$\frac{1}{r^2} \frac{\partial}{\partial r} \left(r^2 \frac{\partial \theta_i}{\partial r} \right) + \frac{2b}{r} = \frac{1}{\alpha_i} \frac{\partial \theta_i}{\partial t}, \quad R_i \leq r \leq r_{o,2} \quad (68)$$

which is subject to:

$$-k_i \frac{\partial \theta_i}{\partial r} \left(r = r_{o,2} \right) = (h_c + h_r) \theta_i \left(r = r_{o,2} \right) \quad (69)$$

$$\theta_i(R_i, t) = 0 \quad (70)$$

$$\theta_i(r_{o,2}, 0) = 0 \quad (71)$$

By applying the separation of variables method, the solution can be written as:

$$\theta_i(r, t) = \sum_{n=1}^{\infty} C_n(t) \left[\frac{\cos(\gamma_n r)}{r} - \cot(\gamma_n R_i) \frac{\sin(\gamma_n r)}{r} \right] \quad (72)$$

Here, γ_n represents the eigenvalues that can be calculated as the roots of the transcendental equation:

$$\tan(\gamma_n r_{o,2}) = \frac{\left(\frac{h_c+h_r}{k_i}\right) r_{o,2} - (\gamma_n r_{o,2}) \cot(\gamma_n R_i) - 1}{\left[\left(\frac{h_c+h_r}{k_i}\right) r_{o,2} \cot(\gamma_n R_i) - \cot(\gamma_n R_i) + (\gamma_n r_{o,2})\right]} \quad (73)$$

As mentioned, R_i is not fixed, so this solution cannot be found in the usual way. In the above equation, both R_i and the eigenvalues γ_n , depend on time. Again discretize in time, with $R_i^k = R_i(t_k)$, $\gamma_{n,k} = \gamma_n(t_k)$, and $C_{n,k} = C_n(t_k)$. Employing the same time approximation, Eq. (68) can be written as follows:

$$\theta_i(r, t_k) - \Delta t \frac{\alpha_i}{r^2} \frac{\partial}{\partial r} \left(r^2 \frac{\partial \theta_i}{\partial r} \right) (r, t_k) = \frac{2 \alpha_i \Delta t b}{r} + \theta_i(r, t_k - \Delta t) \quad (74)$$

where

$$\rho_i l_f (1 - \beta) \frac{R_i^k - R_i^{k-1}}{\Delta t} = k_i \left(\sum_{m=1}^{\infty} C_{m,k} \left[-\frac{(\gamma_{m,k} R_i^k) \sin(\gamma_{m,k} R_i^k) + \cos(\gamma_{m,k} R_i^k)}{(R_i^k)^2} - \cot(\gamma_{m,k} R_i^k) \right. \right. \\ \left. \left. + \frac{(\gamma_{m,k} R_i^k) \cos(\gamma_{m,k} R_i^k) - \sin(\gamma_{m,k} R_i^k)}{(R_i^k)^2} \right] + \frac{(T_a - T_f)}{\left[r_{o,2} - R_i^k + \left(\frac{k_i}{h_c + h_r}\right)\right]} \right) - k_b \sum_{m=1}^{\infty} B_{m,k} \left[\frac{m\pi}{(R_i^k)^2} (-1)^m \right] \quad (80)$$

$$\theta_i(r, t_k) = \sum_{n=1}^{\infty} C_{n,k} \left[\frac{\cos(\gamma_{n,k} r)}{r} - \cot(\gamma_{n,k} R_i^k) \frac{\sin(\gamma_{n,k} r)}{r} \right] \quad (75)$$

and hence

$$\theta_i(r, t_k - \Delta t) = \sum_{n=1}^{\infty} C_{n,k-1} \left[\frac{\cos(\gamma_{n,k-1} r)}{r} - \cot(\gamma_{n,k-1} R_i^{k-1}) \frac{\sin(\gamma_{n,k-1} r)}{r} \right] \quad (76)$$

By substituting Eqs. (75) and (76) into Eq. (74), the following relationship can be obtained:

$$\sum_{n=1}^{\infty} (1 + \Delta t \alpha_i \gamma_{n,k}^2) C_{n,k} \left[\frac{\cos(\gamma_{n,k} r)}{r} - \cot(\gamma_{n,k} R_i^k) \frac{\sin(\gamma_{n,k} r)}{r} \right] = \frac{2 \alpha_i \Delta t b}{r} + \sum_{n=1}^{\infty} C_{n,k-1} \left[\frac{\cos(\gamma_{n,k-1} r)}{r} - \cot(\gamma_{n,k-1} R_i^{k-1}) \frac{\sin(\gamma_{n,k-1} r)}{r} \right] \quad (77)$$

Multiplying by the eigenfunction $\left[\frac{\cos(\gamma_{m,k} r)}{r} - \cot(\gamma_{m,k} R_i^k) \frac{\sin(\gamma_{m,k} r)}{r} \right]$ in Eq. (77) and integrating from R_i^k to $r_{o,2}$, the coefficient of $C_{m,k}$ can be determined as:

$$C_{m,k} = \frac{1}{(1 + \Delta t \alpha_i \gamma_{m,k}^2) I_1} \left[2 \alpha_i \Delta t b I_2 + \sum_{n=1}^{\infty} C_{n,k-1} I_3 \right] \quad (78)$$

where the coefficients I_1 , I_2 and I_3 are computed in the usual way and presented in Appendix A.

Note that the increasing ice domain, with $R_i^k < R_i^{k-1}$, leads to a mismatch in Eq. (77), where the left-hand side should be taken for $R_i^k < r < r_{o,2}$, while the right-hand side is only defined for $R_i^{k-1} < r < r_{o,2}$. Therefore, we extend the solution $\theta_i(r, t_{k-1})$ by zero for $R_i^k < r < R_i^{k-1}$, assuming the water that solidifies between time t_{k-1} and time t_k is at the freezing temperature at t_{k-1} . Similarly, for the initial condition, we take $C_{m,1}$ to be equal to zero for all m , matching $\theta_i(r_{o,2}, 0)$. By computing the coefficients, $C_{m,k}$, the solution for the temperature distribution in the ice shell can be written as follows:

$$\theta_i(r, t_k) = \sum_{m=1}^{\infty} C_{m,k} \left[\frac{\cos(\gamma_{m,k} r)}{r} - \cot(\gamma_{m,k} R_i^k) \frac{\sin(\gamma_{m,k} r)}{r} \right], \quad R_i \leq r \leq r_{o,2} \quad (79)$$

Again, in practice, we truncate the series expansion to approximate θ_i .

To determine the interface radius R_i^k , and complete the specification of the temperature distribution in the water and ice shell, the Stefan condition at the ice-water interface is used. Taking the derivative of Eqs. (65) and (79) and substituting these equations in the Stefan condition (Eq. (35)) along with the approximation $\frac{dR_i}{dt}(t_k) \simeq \frac{R_i^k - R_i^{k-1}}{\Delta t}$, yields the following equation:

It remains to complete the time-stepping procedure by a specification of a time step, Δt , and a way to ensure consistency between the computed solutions for the temperatures, $\theta_i(r, t_k)$ and $\theta_w(r, t_k)$, and the interface radius, R_i^k . To simplify this procedure, we choose Δt by fixing a radial step $\Delta r = R_i^k - R_i^{k-1}$, and solving for the value of Δt that satisfies Eq. (80). Since Δt appears in each of Eqs. (63), (78) and (80), and these all depend on R_i^k in a complicated fashion, this leads to a much simpler iteration than is obtained by fixing Δt and solving for Δr .

Thus, to solve the solidification stage, we first divide the interval $0 < r < r_{o,2}$ into identical steps of size Δr , specifying R_i^k for all k . Then, the time stepping iteration takes the following steps:

- 1) For a chosen number of terms in the series, the eigenvalues (Eq. (73)) are calculated numerically using the bisection method.
- 2) The coefficients $B_{m,k}$ (Eq. (63)) and $C_{m,k}$ (Eq. (78)) are obtained as functions of Δt ,
- 3) Substituting $B_{m,k}$ and $C_{m,k}$ into Eq. (80), Δt is computed, and $t_k = t_{k-1} + \Delta t$,
- 4) After determining Δt , the temperature distribution in the water and the ice shell is obtained explicitly.

This iteration proceeds, for $\frac{r_{o,2}}{\Delta r}$ steps, until $R_i^k = 0$.

3.3. Solution procedure for the solid cooling stage

In the solid cooling stage, again using separation of variables and applying the boundary and initial conditions (Eqs. (41)–(43)), the solution for the temperature distribution is expressed as follows:

$$T_i(r, t) = T_a + \sum_{n=1}^{\infty} D_n \frac{\sin(\xi_n r)}{r} \exp(-\alpha_i \xi_n^2 t) \quad (81)$$

$$\rho_i = \begin{cases} \frac{(1 - v'_a)}{1/\rho_{i,p} - \beta \left(1/\rho_{i,p} - 1/\rho_b\right)}, & S_b < 125\text{‰} \\ \frac{(1 - v'_a)}{1/\rho_{i,p} - \beta S_b \frac{P_3(T_b)}{Q_3(T_b)}}, & S_b \geq 125\text{‰} \end{cases} \quad (85)$$

where α_i is the thermal diffusivity of ice formation,

$$\alpha_i = \frac{k_i}{\rho_i c_i} \quad (82)$$

Here, the coefficients, D_n , are given by:

$$D_n = \frac{\int_0^{r_{o,2}} T_2(r, t_s) \sin(\xi_n r) r dr - T_a \left[\frac{1}{\xi_n} \sin(\xi_n r_{o,2}) - \frac{r_{o,2}}{\xi_n} \cos(\xi_n r_{o,2}) \right]}{\frac{r_{o,2}}{2} - \frac{1}{4\xi_n} \sin 2(\xi_n r_{o,2})} \quad (83)$$

where $T_2(r, t_s)$ is computed from $\theta_i(r, t_s)$ at the time t_s when solidification is completed. The eigenvalues ξ_n , can be determined from the positive roots of the transcendental equation:

$$\tan(\xi_n r_{o,2}) = \frac{\xi_n}{\left(\frac{1}{r_{o,2}} - \frac{(h_c + h_r)}{k_i} \right)} \quad (84)$$

The density of ice formation ρ_i , can be computed by [57,68]: where v'_a is the volume fraction of air in the ice (assumed equal to 0), $\rho_{i,p}$

Table 1
Parameter quantities and correlations used.

Parameter	Quantity/correlation	Units	References
c_a	1005	J/kg.K	[50,73,74]
D_{ab}	$2.227 \times 10^{-5} \left(\frac{T_a + 273}{273} \right)^{1.81}$	m^2/s	[75,76]
k_a	$0.024577 + 9.027 \times 10^{-5} T_a$	W/m.°C	[75,76]
ν_f	3.34×10^5	J/kg	[73]
ν_w	2.27×10^6	J/kg	[73]
P	10^5	Pa	
RH	80	%	
S_w	34	‰	
$T_{0,w}^a$	2	°C	
U	15	m/s	
ν_s	6.17 (12)	m/s (knots)	
α_a	$\frac{1}{(57736 - 585.78 T_a)}$	m^2/s	[75,76]
β	0.34		[57,77,78]
δ^b	110	°	[7]
ϵ	0.95		[46,79]
ϵ	0.622		[80,81]
ν_a	$\frac{1}{(80711.7 - 766.15 T_a)}$	m^2/s	[37]
ρ_d	1027	kg/m ³	[74]
$\rho_{i,p}$	917	kg/m ³	[66,82]
σ	5.67×10^{-8}	W/m ² .K ⁴	

^a Temperature of seawater-surface is generally between -1.7 and 5°C [83].

^b See Cartesian coordinate system in Fig. 1.

is the density of pure ice, and the parameters $P_3(T_b)$ and $Q_3(T_b)$ are two third-degree polynomials in terms of the brine temperature [57,68]:

$$\begin{cases} P_3(T_b) = 8.903 \times 10^{-2} - 1.763 \times 10^{-2} T_b - 5.33 \times 10^{-4} T_b^2 - 8.801 \times 10^{-6} T_b^3 \\ Q_3(T_b) = -4.732 \times 10^3 - 2.245 \times 10^4 T_b - 6.397 \times 10^2 T_b^2 - 10.74 T_b^3 \end{cases} \quad (86)$$

To calculate the thermal conductivity of ice, Maykut and Untersteiner [69] suggested the following model:

$$k_i = 2.03 + 0.117 \frac{S_i}{T} \quad (87)$$

where S_i is the salinity of ice formation given by [41,57]:

$$\beta = \frac{S_i}{S_b} \quad (88)$$

Fichet and Maqueda [70] considered a constant thermal conductivity of sea ice equal to 2.03 W/m.K. The specific heat capacity of ice, c_i , can be determined by [71]:

$$c_i = 0.505 + 0.0018 T + 4.3115 \frac{S_i}{T^2} \quad (89)$$

To estimate the terms in Eqs. (87) and (89), it is assumed that the

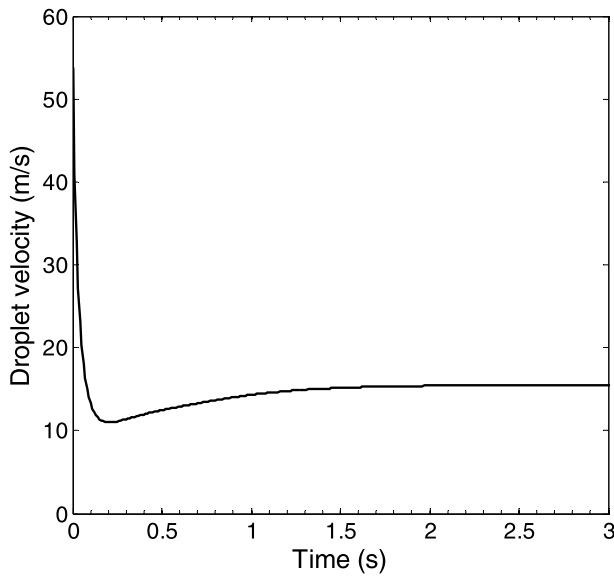


Fig. 4. Changes in the droplet velocity versus time at a wind velocity of 15 m/s and droplet diameter of 1 mm.

temperature is equal to T_f .

In practice, a truncated form of the series solution in Eq. (81) is employed, with 10 terms. The eigenvalues ξ_n , are calculated numerically using the bisection method.

4. Results and discussion

To solve the governing equations to predict the cooling and

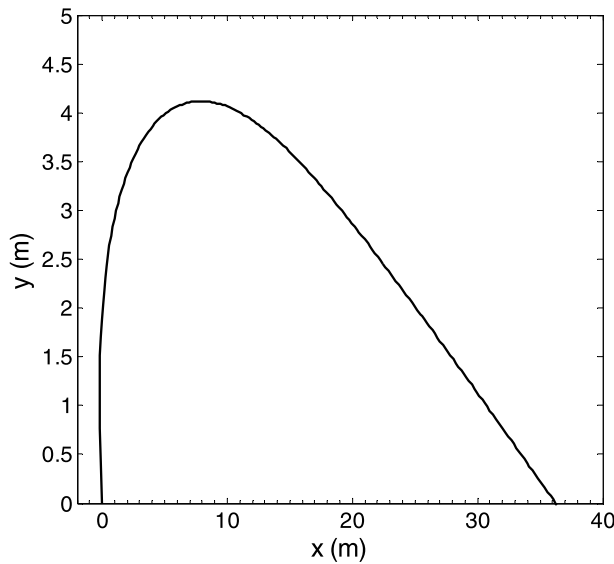


Fig. 5. Trajectory of water droplet with a diameter of 1 mm and wind velocity of 15 m/s during flight on the MFV.

solidification processes and to obtain the temperature distribution within the droplet, several parameters and thermophysical properties are utilized. Some of these parameters are determined by the models presented in the previous sections. Other parameters in the modeling of the droplet processes are given in Table 1. A Matlab [72] code was used in order to perform the simulations.

According to Zakrzewski [84], the typical length of MFVs is 40–50 m. In this paper, an MFV with an overall length of 45 m is selected. It is assumed that the MFV moves directly into the wind and waves, such that a spray cloud will form in front of the MFV (see Fig. 1), and a typical water droplet with a diameter of 1 mm is chosen to analyze the thermal behaviour. It has been reported that small droplets, 1 mm in diameter and smaller, maintain a spherical shape during flight [85,86].

Fig. 4 illustrates the variations of droplet velocity (v_d) over time at a wind velocity of 15 m/s when the water droplet is moving on the MFV. From the figure, the droplet velocity at the initial time is high. With increasing time, the velocity of the droplet decreases until it reaches a minimum at the maximum height in its trajectory. Afterwards, with increasing time, the velocity of the droplet increases until it attains a terminal velocity. As observed in Fig. 4, a water droplet with a diameter of 1 mm attains a terminal velocity after approximately 1.2 s. Fig. 5 indicates the pathway and position of the water droplet throughout its flight over the MFV. As shown in Fig. 5, the water droplet moves in the same direction as the MFV for a very short time after formation at the edge of the vessel, and then turns back towards the deck. The highest height of the droplet in its trajectory is equal to 4.12 m. Additionally, the horizontal position and travel time of the droplet at the moment of impact on the deck are equal to 36.24 m and 1.95 s, respectively. As observed in Figs. 4 and 5, a water droplet with a diameter of 1 mm attains the terminal velocity before impacting on the deck. There is a balance between drag and gravity forces which determines the droplet trajectory during its flight over the MFV. The predicted trajectory of the droplet, illustrated in Fig. 5, shows good agreement with the results obtained by Dehghani et al. [8].

To find the temperature distribution and position of the freezing interface during the solidification stage, as well as to reduce the required computational time, we consider solving the problem by varying the number of terms kept in the series (m) for all stages and for different values of Δr in the solidification stage. As illustrated in Table 2, the difference between the results when keeping more than 6 terms in the series is very small, but to ensure a high accuracy, 10 terms of the series are kept. Choosing a smaller Δr yields more accurate results but requires greater computational cost. In this study, Δr is taken to be 0.01 mm.

Fig. 6 shows the temperature changes over time for the droplet cooling and freezing processes at three different positions: the center ($r = 0$), middle ($r = 0.5r_d$), and surface ($r = r_d$) of the water droplet. As illustrated in Fig. 6(a), the liquid cooling stage is very short and t_f is equal to 0.13 s. The variations of temperature in this stage are non-linear, and the temperature at the droplet's center remains close to the initial droplet temperature. The first ice particles are created on the surface of the water droplet (nucleation) when the droplet's surface temperature attains the freezing temperature. Then, an ice shell forms on the surface, and it moves towards the center of the droplet. Fig. 6(b) depicts the solidification stage from the freezing time ($t_f = 0.13$ s) until solidification is complete ($t_s = 14.04$ s). Furthermore, once the temperature of the droplet's center reaches the freezing temperature, it does not change again until the end of this stage.

Table 2

Comparison of the total droplet freezing time as a function of the number of terms kept in the series (m) and the choice of Δr .

m Δr (mm)	1	2	3	4	5	6	7	8	9	10
0.05	12.32 s	11.39 s	11.13 s	10.98 s	10.89 s	10.83 s	10.79 s	10.76 s	10.74 s	10.72 s
0.01	16.87 s	15.32 s	14.85 s	14.56 s	14.40 s	14.28 s	14.20 s	14.13 s	14.08 s	14.04 s
0.005	18.68 s	17.05 s	16.49 s	16.13 s	15.90 s	15.77 s	15.68 s	15.58 s	15.52 s	15.47 s

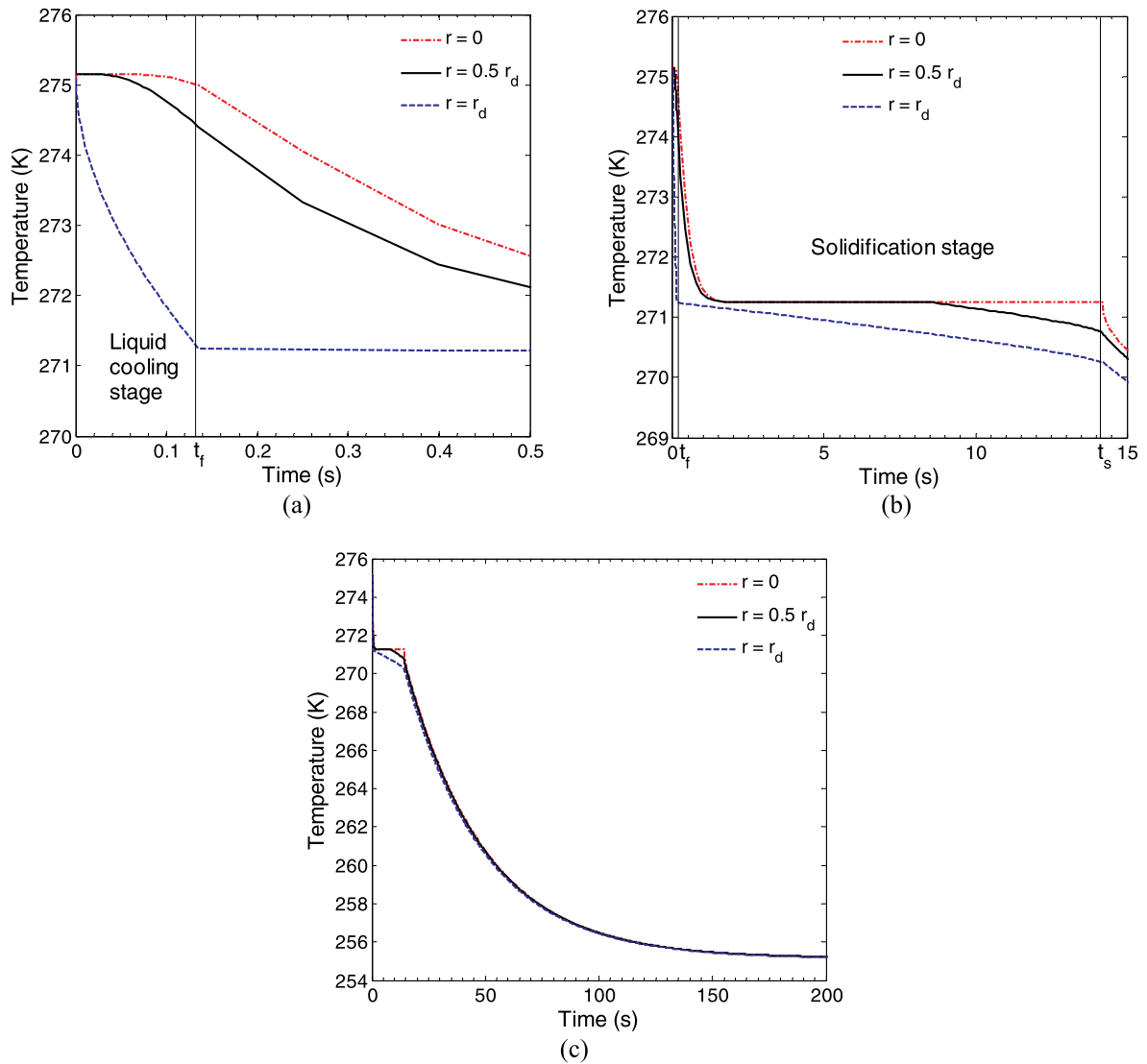


Fig. 6. Droplet cooling and freezing processes: (a) liquid cooling stage, (b) solidification stage, and (c) all stages, ($T_a = -18^\circ\text{C}$, $T_{0,w} = 2^\circ\text{C}$, $U = 15\text{ m/s}$, $Sw = 34\%$ and $RH = 80\%$).

After the solidification stage, the solid cooling stage begins, and the entire droplet (with its salt content) is frozen completely during this stage. As illustrated in Fig. 6(c), the droplet temperature attains the ambient air temperature after approximately 200 s; the temperature changes in this stage are non-linear. According to Fig. 6, there is no supercooling and recalescence stage in the droplet freezing process. This most likely occurs because of high salinity (43‰), high wind velocity (15 m/s), and the existence of a turbulent airflow, so there are insufficient conditions for supercooling. In other words, Fig. 6 shows the cooling curve for the normal freezing of a saline water droplet [87]. It is reported that for several reasons, the phenomenon of supercooling will not occur, or it will happen with a time delay. For example, one reason can be the existence of impurities in water, because the impurities (e.g., salt) decrease the freezing point of water [88] or serve as nucleation sites for crystallization [89]. To model the supercooling phenomenon and find the nucleation temperature in the saline water droplets, if this phenomenon happens, a thermodynamic model is required [90,91]. The theoretical approach presented above does not include this thermodynamic model.

For validation and verification purposes, the results of two cases considered in the present study are compared with the experimental results reported by Hindmarsh et al. [19], as shown in Fig. 7. In case 1 of

the present model, the theoretical approach does not estimate the nucleation temperature. In case 2 of the present model, however, the theoretical approach uses the nucleation temperature (-13.5°C) measured by Hindmarsh et al. [19] from the experimental test. For the theoretical and empirical models in Fig. 7, the temperature profiles are obtained with $T_a = -15^\circ\text{C}$, $T_{0,w} = 7.5^\circ\text{C}$, $U = 0.54\text{ m/s}$, $v_d = 0\text{ m/s}$, $Sw = 0\%$ (freshwater) and $r = 0.78\text{ mm}$ [19]. From Fig. 7, case 1 of the present model shows good agreement, in general, between the theoretical results and the empirical results reported by Hindmarsh et al. [19]. The difference between the theoretical and experimental results is due to: (1) the present model's inability to model the phenomenon of supercooling and determine the nucleation temperature; (2) the difference between some parameters in the empirical test and the theoretical approach (e.g., the Prandtl number, the air viscosity, the air density, and the air thermal conductivity, which have an impact on the Nusselt number and convection heat transfer coefficient, are calculated by different formulae in the theoretical model); (3) acquiring the droplet temperature at $r = 0.5r_d$ in the theoretical solution.

In case 2 of the present model, all data used by Hindmarsh et al. [19] in their experimental test and the nucleation temperature measured from the test, were substituted in the Matlab code and the program was executed. The liquid cooling stage was obtained using the theoretical

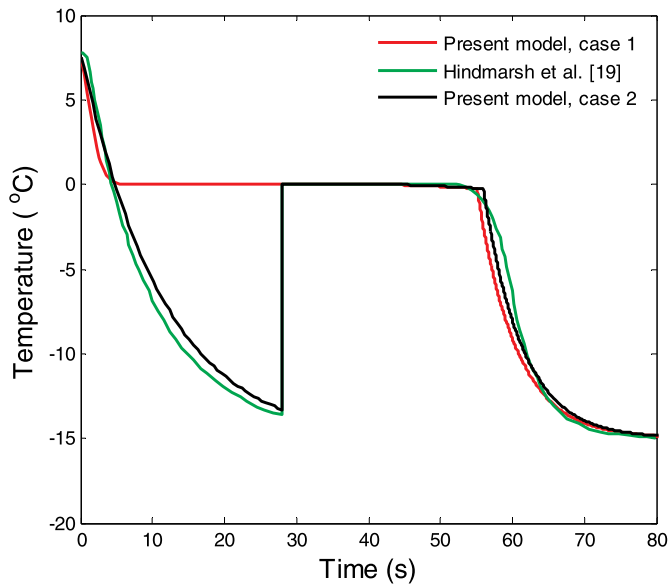


Fig. 7. Comparison of the droplet cooling and freezing processes in two different models for $T_a = -15^\circ$, $T_{0,w} = 7.5^\circ\text{C}$, $S_w = 0\%$ and $U = 0.54\text{ m/s}$. Note that in this figure, the temperature profiles. In our models are plotted at $r = 0.5r_d$.

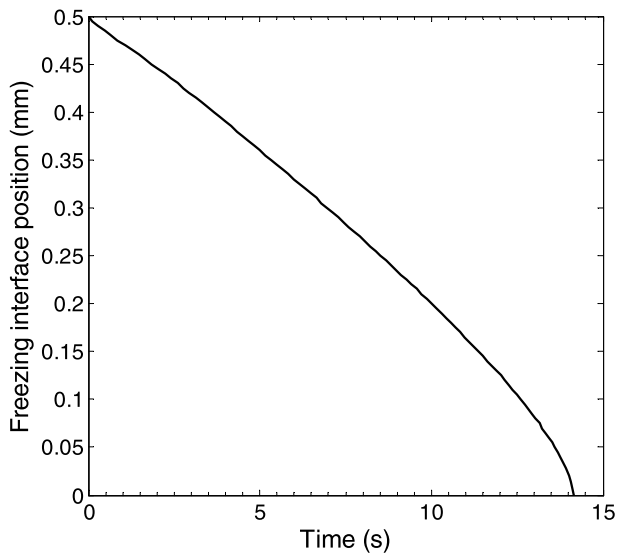


Fig. 8. Variations of the freezing interface position inside the droplet versus time in the solidification stage. For $T_a = -18^\circ\text{C}$, $T_{0,w} = 2^\circ\text{C}$, $U = 15\text{ m/s}$, $S_w = 34\%$ and $RH = 80\%$.

solution until the water was nucleated. Then, to model the recalescence stage, the frozen volume generated from this stage was approximated using a global heat balance. The mass of frozen water is such that the rapidly released latent heat increases the surface temperature of the water droplet from the nucleation temperature (T_n) to the freezing temperature (T_f) [19,92,93]. The volume of frozen droplet, V_i is given by [19]:

$$V_i = V_d \frac{c_w \rho_w}{\rho_i} \frac{(T_f - T_n)}{l_f} \quad (90)$$

The present theoretical model was capable of modeling of the rest of stages. As illustrated in Fig. 7, case 2 of the present model is in good agreement with the empirical results; the difference between them is because of considering a number of parameters in the theoretical model

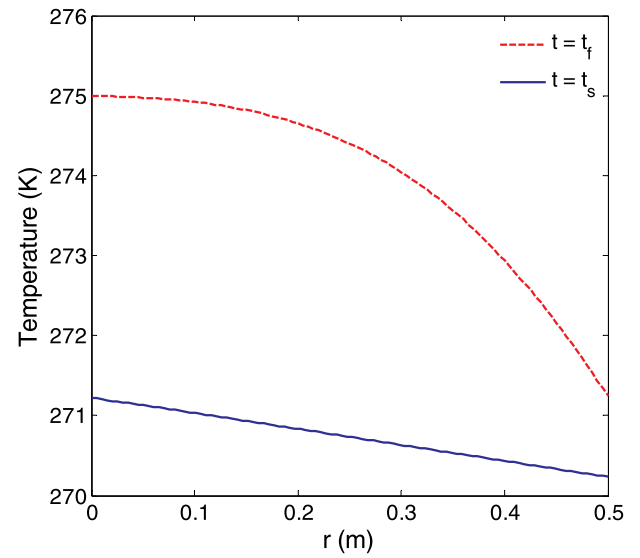


Fig. 9. Temperature distribution within the droplet at the freezing time and solidification time.

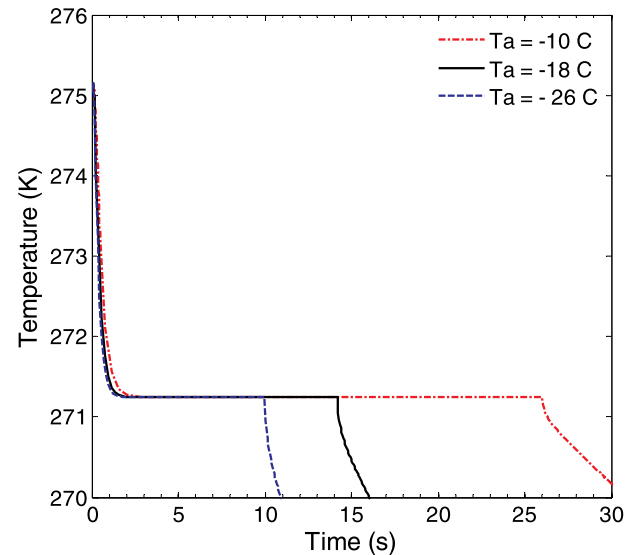


Fig. 10. Changes in the cooling and freezing processes of the droplet at three ambient air temperatures. For $T_{0,w} = 2^\circ\text{C}$, $U = 15\text{ m/s}$, $S_w = 34\%$ and $RH = 80\%$.

that have computed by several formulae, obtaining the droplet temperature at $r = 0.5r_d$ in the theoretical solution, and using an approximation method in the present study. Naterer [94] and Zhang et al. [95–97] reported that the nucleation temperature has a significant impact on the droplet freezing process.

According to Fig. 6, the temperature of the surface and center of the water droplet at the moment of impact on the deck are equal to -2.0°C and -1.9°C , respectively. Fig. 8 shows the changes in the position of the freezing interface from the droplet’s surface over time during the solidification stage. The radius of the freezing interface, R_i , at the moment of impact on the deck (1.95 s) is equal to 0.44 mm. This means that the thickness of the ice shell on the droplet’s surface is equal to 0.06 mm and 12% of the droplet’s volume is ice. Note that Fig. 8 shows that during the solidification stage, the velocity of the inward freezing front within the droplet is almost constant. The temperature distribution inside the droplet at the freezing time (t_f) and solidification time (t_s) are indicated in Fig. 9. As observed in this figure, the distribution of the droplet

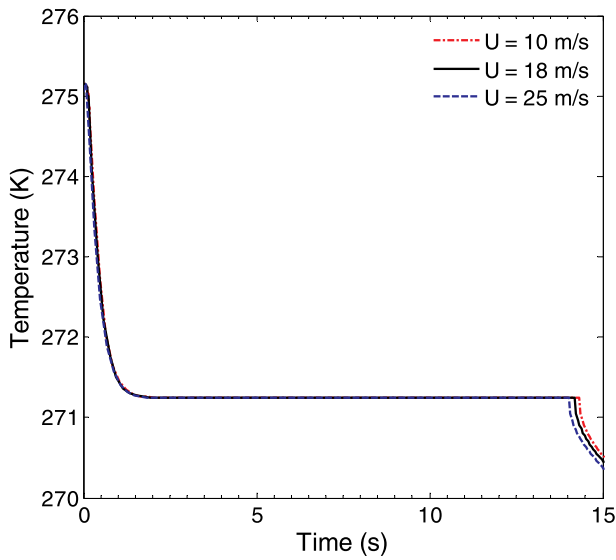


Fig. 11. Changes in the cooling and freezing processes of the droplet at three wind velocities. For $T_a = -18^\circ\text{C}$, $T_{0,w} = 2^\circ\text{C}$, $S_w = 34\%$ and $RH = 80\%$.

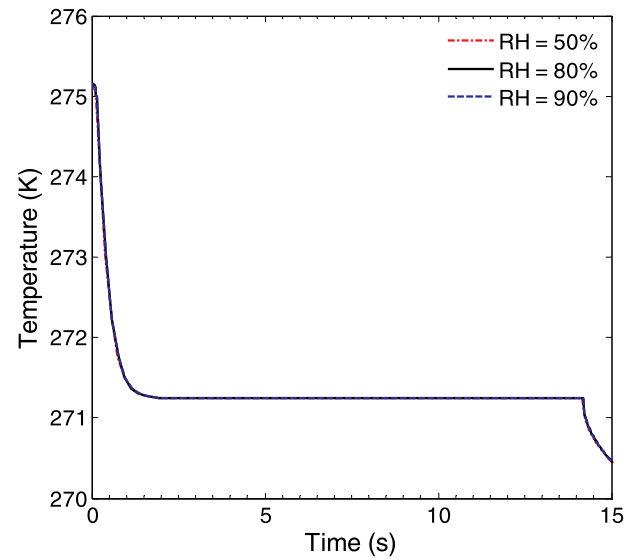


Fig. 13. Changes in the droplet cooling and freezing processes at three relative humidities. For $T_a = -18^\circ\text{C}$, $T_{0,w} = 2^\circ\text{C}$, $U = 15\text{ m/s}$ and $S_w = 34\%$.

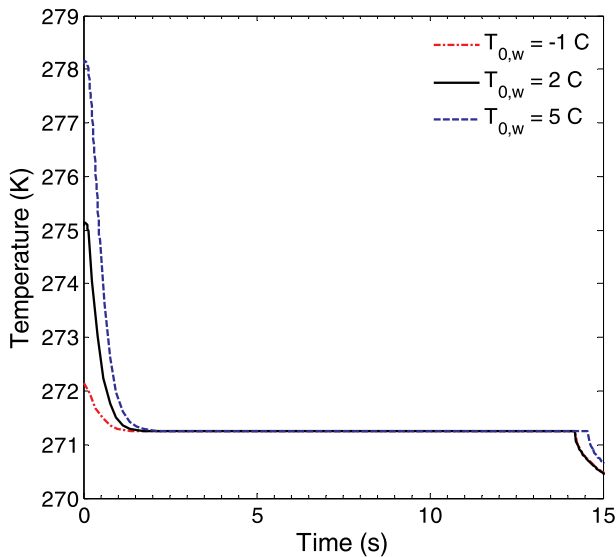


Fig. 12. Changes in the droplet cooling and freezing processes at three initial droplet temperatures. For $T_a = -18^\circ\text{C}$, $U = 15\text{ m/s}$, $S_w = 34\%$ and $RH = 80\%$.

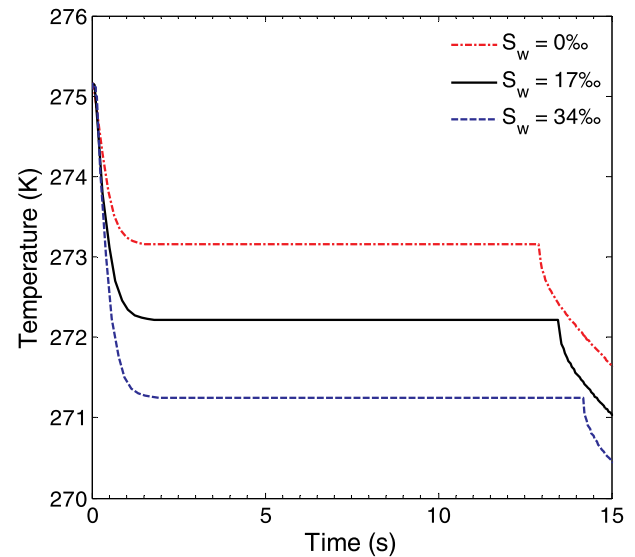


Fig. 14. Changes in the cooling and freezing processes of the droplet at three salinities. For $T_a = -18^\circ\text{C}$, $T_{0,w} = 2^\circ\text{C}$, $U = 15\text{ m/s}$ and $RH = 80\%$.

temperature at the freezing time is non-linear, such that the temperature at the droplet's center is close to the initial droplet temperature and the temperature at the droplet's surface is equal to the freezing temperature. The temperature distribution at the solidification time (t_s) is approximately linear, and the temperature at the droplet's center is equal to the freezing temperature.

An analysis was also conducted to investigate the impact of various input parameters and their variations on the droplet cooling and freezing processes. During each investigation, one parameter is considered variable, while the other parameters are kept constant. Fig. 10 shows the impact of the ambient air temperature on the droplet cooling and freezing processes at the center of the saline water droplet. As illustrated in this figure, the effect of the ambient air temperature on the cooling and freezing processes is significant, so that the liquid cooling and solidification stages take longer when the temperature of the ambient air is increased. In Fig. 10, the solidification time for the ambient air temperatures of -10 , -18 and -26°C are around 26, 14 and 10 s, respectively. This occurs because the temperature of the ambient

air has a notable influence on the heat transfer rate.

Fig. 11 shows the impact of the wind velocity on the droplet cooling and freezing processes at the center of the water droplet. As observed in this figure, although the wind velocity affects the droplet velocity and convection heat transfer coefficient, it has only a slight effect on the cooling and freezing processes, because the droplet velocity reaches a terminal velocity after approximately 1.2 s. The impact of the initial droplet temperature on the droplet cooling and freezing processes at the center of the saline water droplet is shown in Fig. 12. The initial temperature of the droplet has a significant effect on the liquid cooling stage, but the effect of this parameter on the solidification stage is small.

Fig. 13 shows the impact of relative humidity on the droplet cooling and freezing processes at the center of the water droplet. As illustrated in this figure, the effect of relative humidity on the droplet cooling and freezing processes is negligible. It has only a slight effect on the rate of evaporation heat transfer. The impact of salinity on the droplet cooling and freezing processes at the center of the water droplet is illustrated in Fig. 14. As observed in this figure, the salinity has a substantial effect on

the droplet cooling and freezing processes because the freezing temperature, thermal conductivity, density and specific heat capacity are all functions of salinity.

For a constant droplet diameter of 1 mm, the ambient air temperature and salinity have a significant influence on the droplet cooling and freezing processes, whereas the effects of wind velocity, initial droplet temperature and relative humidity are very small. The initial temperature of the droplet has a considerable effect on the liquid cooling stage, but not on the solidification stage.

5. Conclusions

The thermal behaviour and freezing process of a saline water droplet during flight over an MFV in cold weather conditions were investigated and analyzed in this paper by analytical and semi-analytical techniques. To predict and analyze the droplet cooling and freezing processes, three separate stages were considered: a liquid cooling stage, a solidification stage, and a solid cooling stage. A new semi-analytical model was developed to solve the inward moving boundary problem. The results indicate that the liquid cooling stage is very short and the temperature at the center of the water droplet during this stage remains close to the initial temperature of the droplet. Additionally, the temperature changes in this stage are non-linear. During the solidification stage, the velocity of inward freezing in the droplet is approximately constant, and also the variations of temperature are nearly linear when the temperature within the droplet reaches the freezing temperature. The solid cooling stage is much longer compared to other stages, and the variations of temperature in this stage are non-linear. For a case study, theoretical predictions for a droplet with a diameter of 1 mm indicate

the average droplet temperature at the moment of impact on the deck is approximately -1.95°C . Further, there is an ice shell with a thickness of 0.06 mm on the surface of the water droplet at the moment of impact on the deck, and 12% of the volume of the droplet is ice. By analyzing the effect of different parameters on the droplet cooling and freezing processes, it is observed that for a constant droplet diameter of 1 mm, the ambient air temperature and salinity have a substantial influence on the droplet cooling and freezing processes, while the effects of wind velocity, initial droplet temperature, and relative humidity are small.

The proposed approach offers a technique that can be applied in much more general situations than existing analytical methods, which are severely limited by assumptions on model geometry, constant physical parameters, and/or the need for small parameters in a perturbation expansion. At the same time, it offers the typical advantages of an analytical technique with spectral accuracy over numerical techniques that are limited by discretization errors. In principle, by taking more terms in the series expansions and smaller radial steps in the solidification stage, any desired level of accuracy is achievable using the techniques proposed here.

Acknowledgements

The authors gratefully acknowledge the financial support received for this research from Statoil (Norway) (IT03198), Research and Development Corporation of Newfoundland and Labrador (RDC), MITACS (IT03198), Petroleum Research of Newfoundland & Labrador (PRNL) (IT03198), American Bureau of Shipping (ABS) (207095), and the NSERC Discovery Grant program.

Appendix A

As mentioned in subsection 3.2, multiplying by the eigenfunction $\left[\frac{\cos(\gamma_{m,k} r)}{r} - \cot(\gamma_{m,k} R_i^k) \frac{\sin(\gamma_{m,k} r)}{r} \right]$ in Eq. (77) and integrating from R_i^k to $r_{o,2}$, the coefficients $C_{m,k}$ (Eq. (78)) can be determined. In this equation, the coefficients I_1 , I_2 and I_3 are obtained from the relationships below:

$$I_1 = \frac{1}{2} (r_{o,2} - R_i^k) + \frac{1}{4\gamma_{m,k}} [\sin 2(\gamma_{m,k} r_{o,2}) - \sin 2(\gamma_{m,k} R_i^k)] + \frac{1}{2\gamma_{m,k}} \cot(\gamma_{m,k} R_i^k) [\cos 2(\gamma_{m,k} r_{o,2}) - \cos 2(\gamma_{m,k} R_i^k)] \\ + \cot^2(\gamma_{m,k} R_i^k) \left\{ \frac{1}{2} (r_{o,2} - R_i^k) - \frac{1}{4\gamma_{m,k}} [\sin 2(\gamma_{m,k} r_{o,2}) - \sin 2(\gamma_{m,k} R_i^k)] \right\} \quad (91)$$

$$I_2 = \frac{1}{\gamma_{m,k}} [\sin(\gamma_{m,k} r_{o,2}) - \sin(\gamma_{m,k} R_i^k)] + \frac{1}{\gamma_{m,k}} \cot(\gamma_{m,k} R_i^k) [\cos(\gamma_{m,k} r_{o,2}) - \cos(\gamma_{m,k} R_i^k)] \quad (92)$$

$$I_3 = E_1 - \cot(\gamma_{m,k} R_i^k) E_2 - \cot(\gamma_{n,k-1} R_i^{k-1}) E_3 + \cot(\gamma_{n,k-1} R_i^{k-1}) \cot(\gamma_{m,k} R_i^k) E_4 + T_f E_5 - T_f \cot(\gamma_{m,k} R_i^k) E_6 \quad (93)$$

In Eq. (91), E_1 to E_6 are given as follows:

$$E_1 = \frac{1}{2(\gamma_{n,k-1} - \gamma_{m,k})} [\sin(\gamma_{n,k-1} - \gamma_{m,k}) r_{o,2} - \sin(\gamma_{n,k-1} - \gamma_{m,k}) R_i^{k-1}] \\ + \frac{1}{2(\gamma_{n,k-1} + \gamma_{m,k})} [\sin(\gamma_{n,k-1} + \gamma_{m,k}) r_{o,2} - \sin(\gamma_{n,k-1} + \gamma_{m,k}) R_i^{k-1}] \quad (94)$$

$$E_2 = -\frac{1}{2(\gamma_{n,k-1} + \gamma_{m,k})} [\cos(\gamma_{n,k-1} + \gamma_{m,k}) r_{o,2} - \cos(\gamma_{n,k-1} + \gamma_{m,k}) R_i^{k-1}] \\ + \frac{1}{2(\gamma_{n,k-1} - \gamma_{m,k})} [\cos(\gamma_{n,k-1} - \gamma_{m,k}) r_{o,2} - \cos(\gamma_{n,k-1} - \gamma_{m,k}) R_i^{k-1}] \quad (95)$$

$$E_3 = -\frac{1}{2(\gamma_{n,k-1} + \gamma_{m,k})} [\cos(\gamma_{n,k-1} + \gamma_{m,k}) r_{o,2} - \cos(\gamma_{n,k-1} + \gamma_{m,k}) R_i^{k-1}] \\ - \frac{1}{2(\gamma_{n,k-1} - \gamma_{m,k})} [\cos(\gamma_{n,k-1} - \gamma_{m,k}) r_{o,2} - \cos(\gamma_{n,k-1} - \gamma_{m,k}) R_i^{k-1}] \quad (96)$$

$$E_4 = \frac{1}{2(\gamma_{n,k-1} - \gamma_{m,k})} [\sin(\gamma_{n,k-1} - \gamma_{m,k}) r_{o,2} - \sin(\gamma_{n,k-1} - \gamma_{m,k}) R_i^{k-1}] - \frac{1}{2(\gamma_{n,k-1} + \gamma_{m,k})} [\sin(\gamma_{n,k-1} + \gamma_{m,k}) r_{o,2} - \sin(\gamma_{n,k-1} + \gamma_{m,k}) R_i^{k-1}] \quad (97)$$

$$E_5 = \left[\frac{R_i^{k-1}}{\gamma_{m,k}} \sin(\gamma_{m,k} R_i^{k-1}) + \frac{1}{\gamma_{m,k}^2} \cos(\gamma_{m,k} R_i^{k-1}) \right] - \left[\frac{R_i^k}{\gamma_{m,k}} \sin(\gamma_{m,k} R_i^k) + \frac{1}{\gamma_{m,k}^2} \cos(\gamma_{m,k} R_i^k) \right] \quad (98)$$

$$E_6 = \left[-\frac{R_i^{k-1}}{\gamma_{m,k}} \cos(\gamma_{m,k} R_i^{k-1}) + \frac{1}{\gamma_{m,k}^2} \sin(\gamma_{m,k} R_i^{k-1}) \right] - \left[-\frac{R_i^k}{\gamma_{m,k}} \cos(\gamma_{m,k} R_i^k) + \frac{1}{\gamma_{m,k}^2} \sin(\gamma_{m,k} R_i^k) \right] \quad (99)$$

References

- [1] C.W. Chan, F.L. Tan, Solidification inside a sphere - an experimental study, *Int. Commun. Heat Mass Transf.* 33 (2006) 335–341.
- [2] S. Tabakova, F. Feuillebois, S. Radev, Freezing of a supercooled spherical droplet with mixed boundary conditions, *Proc. R. Soc. A* 466 (2010) 1117–1134.
- [3] Nai-Yi Li, J.R. Barber, Sinusoidal perturbation solutions for planar solidification, *Int. J. Heat Mass Transf.* 32 (5) (1989) 935–941.
- [4] S.C. Gupta, P.R. Arora, Analytical and numerical solutions of inward spherical solidification of a superheated melt with radiative-convective heat transfer and density jump at freezing front, *Warme-Stoffubetr.* 27 (1992) 377–384.
- [5] J.M. Hill, A. Kucera, Freezing a saturated liquid inside a sphere, *Int. J. Heat Mass Transf.* 26 (11) (1983) 1631–1637.
- [6] M. Parang, D.S. Crocker, B.D. Haynes, Perturbation solution for spherical and cylindrical solidification by combined convective and radiative cooling, *Int. J. Heat Fluid Flow* 11 (2) (1990) 142–148.
- [7] S.R. Dehghani, Y.S. Muzychka, G.F. Naterer, Droplet trajectories of wave-impact sea spray on a marine vessel, *Cold Reg. Sci. Technol.* 127 (2016) 1–9.
- [8] S.R. Dehghani, G.F. Naterer, Y.S. Muzychka, Droplet size and velocity distributions of wave-impact sea spray over a marine vessel, *Cold Reg. Sci. Technol.* 132 (2016) 60–67.
- [9] A.R. Dehghani-Sanij, Y.S. Muzychka, G.F. Naterer, Analysis of ice accretion on vertical surfaces of marine vessels and structures in Arctic conditions, in: *The ASME 2015 34th International Conference on Ocean, Offshore and Arctic Engineering (OMAE2015)*, OMAE2015-41306, St. John's, Newfoundland, Canada, 2015.
- [10] A.R. Dehghani-Sanij, Y.S. Muzychka, G.F. Naterer, Predicted ice accretion on horizontal surfaces of marine vessels and offshore structures in Arctic regions, in: *The ASME 2016 35th International Conference on Ocean, Offshore and Arctic Engineering (OMAE2016)*, OMAE2016-54054, Busan, South Korea, 2016.
- [11] A.R. Dehghani-Sanij, S.R. Dehghani, G.F. Naterer, Y.S. Muzychka, sea spray icing phenomena on marine vessels and offshore structures: review and formulation, *Ocean Eng.* 132 (2017) 25–39.
- [12] A.R. Dehghani-Sanij, S.R. Dehghani, G.F. Naterer, Y.S. Muzychka, Marine icing phenomena on vessels and offshore structures: prediction and analysis, *Ocean Eng.* 143 (2017) 1–23.
- [13] A.R. Dehghani-Sanij, G.F. Naterer, Y.S. Muzychka, Heat transfer of impinging seawater spray and ice accumulation on marine vessel surfaces, *Heat Transf. Res.* 48 (17) (2017) 1599–1624.
- [14] A. Bodaghkhani, S.R. Dehghani, Y.S. Muzychka, B. Colbourne, Understanding spray cloud formation by wave impact on marine objects, *Cold Reg. Sci. Technol.* 129 (2016) 114–136.
- [15] A.R. Dehghani-Sanij, M. Mahmoodi, S.R. Dehghani, G.F. Naterer, Y.S. Muzychka, Experimental investigation of vertical marine surface icing in periodic spray and cold conditions, *J. Offshore Mech. Arct. Eng. (OMAE)* 141 (2019), 021502, 1–021502-16.
- [16] H.S. Carslaw, J.G. Jaeger, *Conduction of Heat in Solids*, second ed., Oxford University Press, 1959, p. 285.
- [17] T.G. Krzewinski, R.G. Tart, *Thermal Design Considerations in Frozen Ground Engineering: A State of the Practice Report*, American Society of Civil Engineers (ASCE), New York, USA, 1985.
- [18] H.J. Schulze, P.M. Beckett, J.A. Howarth, G. Poots, Analytical and numerical solutions to two-dimensional moving interface problems with applications to the solidification of killed steel ingots, *Proc. R. Soc. A* 383 (1983) 313–343.
- [19] J.P. Hindmarsh, A.B. Russell, X.D. Chen, Experimental and numerical analysis of the temperature transition of a suspended freezing water droplet, *Int. J. Heat Mass Transf.* 46 (2003) 1199–1213.
- [20] W.D. Murray, F. Landis, Numerical and machine solutions of transient heat-conduction problems involving melting or freezing, *Trans. ASME J. Heat Transf.* 81 (1959) 106–112.
- [21] V. Voller, Implicit finite-difference solutions of the enthalpy formulation of stefan problems, *J. Numer. Anal.* 5 (1985) 201–214.
- [22] J. Caldwell, C. Chan, Spherical solidification by the enthalpy method and the heat balance integral method, *Appl. Math. Model.* 24 (2000) 45–53.
- [23] A. Bonaccina, Numerical solution of phase-change problems, *Int. J. Heat Mass Transf.* 16 (1973) 1825–1832.
- [24] G. Wang, E. Matthys, Numerical modeling of phase change and heat transfer rapid solidification processes: use of control volume integrals with element subdivision, *Int. J. Heat Mass Transf.* 35 (1992) 141–153.
- [25] A. Wheeler, N. Ahmad, Recent developments in phase field models of solidification, *Adv. Space Res.* 16 (7) (1995) 163–172.
- [26] S.C. Gupta, Analytical and numerical solutions of radially symmetric inward solidification problems in spherical geometry, *Int. J. Heat Mass Transf.* 30 (12) (1987) 2611–2616.
- [27] R.I. Pedroso, G.A. Domoto, Inward spherical solidification-solution by the method of strained coordinates, *Int. J. Heat Mass Transf.* 16 (1973) 1037–1043.
- [28] R.I. Pedroso, G.A. Domoto, Perturbation solutions for spherical solidification of saturated liquids, *ASME J. Heat Transf.* 95 (1973) 42–46.
- [29] R.V. Seeniraj, T.K. Bose, Planar solidification of a warm flowing liquid under different boundary conditions, *Warme-Stoffubetr.* 16 (1982) 105–111.
- [30] S. Weinbaum, L.M. Jiji, Singular perturbation theory for melting or freezing in finite domains initially not at the fusion temperature, *J. Appl. Mech.* 44 (1977) 25–30.
- [31] M.M. Yan, P.N.S. Huang, Perturbation solutions to phase change problems subjected to convection and radiation, *Trans. ASME J. Heat Transf.* 96 (1974) 95–100.
- [32] L.F. Milanez, J.L. Boldrini, Perturbation solution for spherical solidification by convective cooling, *J. Thermophys. Heat Transf.* 2 (1988) 88–91.
- [33] C.L. Huang, Y.P. Shih, A perturbation method for spherical and cylindrical solidification, *Chem. Eng. Sci.* 30 (1975) 897–906.
- [34] D.S. Riley, F.T. Smith, G. Poots, The inward solidification of spheres and circular cylinders, *Int. J. Heat Mass Transf.* 17 (1974) 1507–1516.
- [35] F. Feuillebois, A. Lasek, P. Creismas, F. Pigeonneau, A. Szaniawski, Freezing of a subcooled liquid droplet, *J. Colloid Interface Sci.* 169 (1995) 90–102.
- [36] A.L. London, R.A. Seban, Rate of ice formation, *Trans. Am. Soc. Mech. Eng.* 65 (7) (1943) 771–779.
- [37] J.P. Zarling, *Heat and Mass Transfer from Freely Falling Drops at Low Temperatures*, US Army Cold Regions Research and Engineering Laboratory, 1980. CRREL Report BO-1B.
- [38] J.P. Hindmarsh, A.B. Russell, X.D. Chen, Experimental and numerical analysis of the temperature transition of a freezing food solution droplet, *Chem. Eng. Sci.* 59 (2004) 2503–2515.
- [39] M. Tagami, M. Hamai, I. Mogi, K. Watanabe, M. Motokawa, Solidification of levitating water in a gradient strong magnetic field, *J. Cryst. Growth* 203 (1999) 594–598.
- [40] W. Gao, D. Smith, D. Sego, Freezing behavior of freely suspended industrial waste droplets, *Cold Reg. Sci. Technol.* 31 (2000) 13–26.
- [41] A. Kulyakhtin, A. Tsarau, A time-dependent model of marine icing with application of computational fluid dynamics, *Cold Reg. Sci. Technol.* 104–105 (2014) 33–44.
- [42] E.P. Lozowski, K. Szilder, L. Makkonen, Computer simulation of marine ice accretion, *R. Soc. Lond. Philos. Trans. Ser. A* 358 (2000) 2811–2845.
- [43] L. Makkonen, Models for the growth of rime, glaze, icicles and wet snow on structures, *Phil. Trans. R. Soc. Lond. A* 358 (2000) 2913–2939.
- [44] P. Fu, M. Farzaneh, G. Bouchard, Two-dimensional modelling of the ice accretion process on transmission line wires and conductors, *Cold Reg. Sci. Technol.* 46 (2006) 132–146.
- [45] A. Kulyakhtin, O. Shipilova, M. Muskulus, Numerical simulation of droplet impingement and flow around a cylinder using RANS and LES, *J. Fluids Struct.* 48 (2014) 280–294.
- [46] G. Lorenzini, O. Saro, Thermal fluid dynamic modelling of water droplet evaporation in air, *Int. J. Heat Mass Transf.* 62 (2013) 323–335.
- [47] A.R. Dehghani-Sanij, G.F. Naterer, Y.S. Muzychka, K. Pope, Thermal Analysis of Saline Droplet Motion with Cooling in Cold Regions, the ASME 2017 36th International Conference on Ocean, Offshore and Arctic Engineering (OMAE2017), OMAE2017-61097, Trondheim, Norway, 2017.
- [48] A.R. Dehghani-Sanij, Y.S. Muzychka, G.F. Naterer, Droplet trajectory and thermal analysis of impinging saline spray flow on marine platforms in cold seas and ocean regions, *Ocean Eng.* 148 (2018) 538–547.
- [49] R. Clift, J.R. Grace, M.E. Weber, *Bubbles, Drops and Particles*, Academic Press, San Diego, Calif., 1978.

- [50] C.R. Tracy, W.R. Welch, W.P. Porter, Properties of air, in: *A Manual for Use in Biophysical Ecology*, third ed., University of Wisconsin, 1980. Technical report No. 1.
- [51] T.L. Bergman, A.S. Lavine, F.P. Incropera, D.P. DeWitt, *Introduction to Heat Transfer*, sixth ed., John Wiley & Sons, Inc, 2011.
- [52] T.G. Myers, Extension to the messinger model for aircraft icing, *AIAA J.* 39 (2) (2001) 211–218.
- [53] W.E. Ranz, W.R. Marshall, Evaporation from drops, *Chem. Eng. Prog.* 48 (3) (1952) 141–146.
- [54] M.H. Sadafi, I. Jahn, A.B. Stilgoe, K. Hooman, Theoretical and experimental studies on a solid containing water droplet, *Int. J. Heat Mass Transf.* 78 (2015) 25–33.
- [55] M.H. Sadafi, I. Jahn, A.B. Stilgoe, K. Hooman, A theoretical model with experimental verification for heat and mass transfer of saline water droplets, *Int. J. Heat Mass Transf.* 81 (2014) 1–9.
- [56] M. Mezhericher, A. Levy, I. Borde, Heat and mass transfer of single droplet/wet particle drying, *Chem. Eng. Sci.* 63 (1) (2008) 12–23.
- [57] I. Horjen, Numerical modeling of two-dimensional sea spray icing on vessel-mounted cylinders, *Cold Reg. Sci. Technol.* 93 (2013) 20–35.
- [58] L. Makkonen, Solid fraction in dendritic solidification of a liquid, *Appl. Phys. Lett.* 96 (9) (2010), 091910, 1–091910-3.
- [59] L. Makkonen, Salinity and growth of ice formed by sea spray, *Cold Reg. Sci. Technol.* 14 (1987) 163–171.
- [60] T. Forest, E. Lozowski, R. Gagnon, Estimating Marine Icing on Offshore Structures Using RIGICE04, *International Workshop on Atmospheric Icing on Structures (IWAIS)*, Canada, Montreal, 2005.
- [61] A. Assur, Composition of sea ice and its tensile strength, in: *Arctic Sea Ice*, vol. 598, U.S. National Academic Sciences-National Research Council, Pub., 1958, pp. 106–138.
- [62] E.L. Andreas, Time constants for the evolution of sea spray droplets, *Tellus B* 42 (5) (1990) 481–497.
- [63] P. Schwerdtfeger, The thermal properties of sea ice, *J. Glaciol.* 4 (36) (1963) 789–807.
- [64] M.N. Ozisik, *Heat Conduction*, John Wiley, New York, 2000.
- [65] N.A. Lange, G.M. Forke, *Handbook of Chemistry*, eighth ed., Handbook Publ., Sandusky, Ohio, USA, 1952.
- [66] D.J. Pringle, H. Eicken, H.J. Trodahl, L.G.E. Backstrom, Thermal Conductivity of Landfast Antarctic and Arctic Sea Ice, *J. Geoph. Research* C04017, 112 (2007) 1–13.
- [67] S. Kuwahara, Velocity of sound in sea water and calculation of the velocity for use in sonic sounding, *Jpn. J. Astron. Geophys.* 16 (1938).
- [68] G.F.N. Cox, W.F. Weeks, Equations for determining the gas and brine volumes of sea-ice samples, *J. Glaciol.* 29 (102) (1983) 306–316.
- [69] G. Maykut, N. Untersteiner, Some results from a time-dependent thermodynamic model of sea ice, *J. Geophys. Res.* 76 (1971) 1550–1576.
- [70] T. Fichefet, M.M. Maqueda, Sensitivity of a global sea ice model to the treatment of ice thermodynamics and dynamics, *J. Geophys. Res.* 102 (12) (1997) 609–646.
- [71] N. Ono, Specific heat and fusion of sea ice, *Inst. of Low Temp. Sci.*, in: H. Oura (Ed.), *Physics of Snow and Ice: International Conference on Low Temperature Science*, vol. 1 Hokkaido Univ., Sapporo, Japan, 1967, pp. 599–610, 1
- [72] *Matlab Version R14*, The MathWorks Inc., USA.
- [73] E. Schröder Hansen, Numerical Modeling of Marine Icing on Offshore Structures and Vessels, MS Thesis, Department of Physics, Norwegian University of Science and Technology, Trondheim, Norway, 2012.
- [74] *Engineering Toolbox*, 2017. Retrieved from, <http://www.engineeringtoolbox.com>.
- [75] *ASHRAE Handbook of Fundamental*, American Society of Heating, Refrigerating and Air Conditioning Engineers, Inc., New York, NY, 1977.
- [76] B.V. Karlekar, R.M. Desmond, *Engineering Heat Transfer*, West Publishing Co., New York, 1977.
- [77] I. Horjen, Offshore drilling rig ice accretion modeling including a surficial brine film, *Cold Reg. Sci. Technol.* 119 (2015) 84–110.
- [78] I. Horjen, Numerical Modeling of Time-dependent Marine Icing, Anti-icing and Deicing, Doctoral Thesis, Norges Tekniske Hogskole (NTH), Trondheim, Norway, 1990.
- [79] G. Guglielmini, C. Pisoni, *Introduzione Alla Trasmissione Del Calore*, Casa Editrice Ambrosiana, Milano, 2001 (in Italian).
- [80] R. Kato, Modeling of Ship Superstructure Icing: Application to Ice Bridge Simulators, Department of Marine Technology, Norwegian University of Science and Technology, Trondheim, Norway, 2012. MS thesis.
- [81] L. Makkonen, Estimation of wet snow accretion on structures, *Cold Reg. Sci. Technol.* 17 (1989) 83–88.
- [82] T.W. Brakel, J.P.F. Charpin, T.G. Myers, One-dimensional ice growth due to incoming supercooled droplets impacting on a thin conducting substrate, *Int. J. Heat Mass Transf.* 50 (2007) 1694–1705.
- [83] *Environment and Climate Change, Canada, Met 101*. Retrieved from: <http://www.ec.gc.ca/meteo-weather/default.asp?lang=En&n=279AC7ED-1&offset=6&toc=show>.
- [84] W.P. Zakrzewski, *Icing of Ships, Part I: Splashing a Ship with Spray*, vol. 66, NOAA Technical Memorandum, ERL PMEL, Seattle, 1986, p. 74.
- [85] J.E. McDonald, The shape and aerodynamics of large rain drops, *J. Meteorol.* 11 (1954) 478–494.
- [86] A.R. Dehghani-Sanij, Theoretical and Experimental Study of Heat Loss and Ice Accretion from Large Structures on the Marine Vessels and Offshore Structures, PhD Thesis, Memorial University of Newfoundland (MUN), St John's, NL, Canada, 2017.
- [87] V. Alexiades, A.D. Solomon, *Mathematical Modeling of Melting and Freezing Processes*, first ed., CRC Press, 1992.
- [88] J.A. Evans (Ed.), *Frozen Food Science and Technology*, first ed., Wiley-Blackwell, 2008.
- [89] S. Martin, Frazil ice in rivers and oceans, *Annu. Rev. Fluid Mech.* 13 (1981) 379–397.
- [90] J.W.P. Schmelzer, A.S. Abyzov, E.B. Ferreira, V.M. Fokin, Curvature dependence of the surface tension and crystal nucleation in liquids, *Int. J. Appl. Glass Sci.* 10 (2019) 57–68.
- [91] K.K. Tanaka, Y. Kimura, Theoretical analysis of crystallization by homogeneous nucleation of water droplets, *Phys. Chem. Phys.* 21 (2019) 2410–2418.
- [92] F. Feuillebois, A. Lasek, P. Creisemeas, F. Pigeonneau, A. Szaniawski, Freezing of a subcooled liquid droplet, *J. Colloid Interface Sci.* 169 (1995) 90–102.
- [93] X. Chen, P. Chen, Freezing of aqueous solution in a simple apparatus designed for measuring freezing point, *Food Res. Int.* 29 (8) (1996) 723–729.
- [94] G.F. Naterer, *Advanced Heat Transfer*, second ed., CRC Press, Boca Raton, FL, 2018.
- [95] X. Zhang, X. Wu, J. Min, X. Liu, Modelling of sessile water droplet shape evolution during freezing with consideration of supercooling effect, *Appl. Therm. Eng.* 125 (2017) 644–651.
- [96] X. Zhang, X. Liu, X. Wu, J. Min, Simulation and experiment on supercooled sessile water droplet freezing with special attention to supercooling and volume expansion effects, *Int. J. Heat Mass Transf.* 127 (Part A) (2018) 975–985.
- [97] X. Zhang, X. Liu, X. Wu, J. Min, Experimental investigation and statistical analysis of icing nucleation characteristics of sessile water droplets, *Exp. Therm. Fluid Sci.* 99 (2018) 26–34.